Should Torroja's prestressed concrete Alloz aqueduct be thought of as a beam or a shell?

Engineering Structures 264 (2022) 114425

Contents lists available at ScienceDirect

Engineering Structures

journal homepage: www.elsevier.com/locate/engstruct

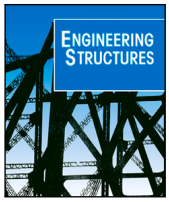

Should Torroja's prestressed concrete Alloz aqueduct be thought of as a beam or a shell?

Alexander Sehlström *, Karl-Gunnar Olsson, Chris J.K. Williams

Department of Architecture and Civil Engineering, Chalmers University of Technology, Sweden

ARTICLE INFO

Keywords:
Eduardo Torroja
Prestress
Aqueduct
Cylindrical membrane shell
Euler–Bernoulli beam

ABSTRACT

This paper examines the structural action of Eduardo Torroja's Alloz aqueduct, completed in 1939, to see whether we should think of it as acting as a beam or a shell. This is of interest regarding the Alloz aqueduct itself, but also in the design of similar structures in the future, where we must have a simple conceptual understanding of how we want it to work.

We apply two alternative approaches available at that time, before computers. Firstly, the membrane theory of shells, effectively assuming the aqueduct walls are infinitely flexible in bending, and secondly, the Euler–Bernoulli 'plane sections remain plane' elementary beam theory. We also review Torroja's calculations which were based on an elaboration of the Euler–Bernoulli beam theory know as the Griffith–Taylor theory for the bending of cantilevers, although we are uncertain as to why he decided to use the Griffith–Taylor theory for a thin walled structure.

Both the membrane shell and Euler–Bernoulli beam theory require a prestress to be applied along the longitudinal edges of the channel. However, the level of prestress in the Alloz aqueduct is consistent with the beam theory, which seams the most appropriate approach.

Whether or not a structure of this type acts as a shell depends upon the thickness of the wall. The thinner the wall, the more it act as a shell. The wall thickness of the Alloz aqueduct is sufficient for it to act mainly as a beam.

1. Introduction

It is important that engineers should understand how structures carry loads using relatively simple conceptual models, both during initial design and in performing independent checks of a computer analysis. Computer analysis potentially gives accurate results, but they only make real sense to us if we have a physical understanding of what is going on. The lower bound or safe theorem of plasticity [1,2] tells us that a sufficiently ductile structure will be safe if we can find a state of stress in equilibrium that does not violate yield. So even though serviceability criteria such as deflections and cracking are of importance, the prevention of collapse is ensured by designing a ductile structure that can satisfy equilibrium, even if we do not know what actual stresses will occur. In fact, materials such as concrete are non-linear elastic and subject to creep, meaning results from a linear-elastic computer analysis will not be that accurate anyway.

Here we examine a slightly simplified geometry of Eduardo Torroja's prestressed concrete Alloz aqueduct completed in northeast Spain in 1939. We consider which simple theoretical approach best captures the structural behaviour: the Euler–Bernoulli 'plane sections remain plane' elementary beam theory or the membrane theory of shells. Of course, there is also the bending theory of shells, but that is very complex and leads to equations that are difficult to solve, so one instead uses the finite element method with elements based on the bending theory of shells.

We know that the Euler–Bernoulli theory and the membrane theory satisfy equilibrium and that if the walls of a structure are very stiff in bending, the behaviour will be near the Euler–Bernoulli theory, but if the walls are very flexible, the behaviour will be near the membrane theory.

We review Torroja's actual calculations for the project, which are based on an elaboration of the Euler–Bernoulli beam theory known as the Griffith–Taylor theory for the bending of cantilevers.

1.1. Eduardo Torroja

Eduardo Torroja (1899–1961) was one of the most creative and important structural engineers of the 20th century [3] and became well known beyond the world of engineering for his mastery of reinforced concrete and brickwork [4], often in extraordinary architectural

* Corresponding author.
E-mail address: alexander.sehlstrom@chalmers.se (A. Sehlström).

https://doi.org/10.1016/j.engstruct.2022.114425
Received 2 June 2021; Received in revised form 27 February 2022; Accepted 15 May 2022
Available online 27 May 2022

forms [5]. He was professor at the Civil Engineering School of Madrid 1939–1961 and co-founded in 1949 the Spanish Prestressed Concrete Association, in 1952 the Féderation Internationale de la Précontrainte (FIP), and in 1953 the Comité Européen du Béton (CEB) [6]; later, in 1998, FIP and CEB merged into the International Federation for Structural Concrete *fib*. In 1959, he founded the International Association for Shell and Spatial Structures (IASS) [7].

To develop his construction technologies, Torroja built scale models (see e.g. [8,9]) and monitored his structures to check their safety, learn about their structural behaviour, and improve later designs [10]. His explorations resulted in some of the most innovative structures of their kind, such as the shells of the Algeciras Market [11], Madrid hippodrome [12,13], and Frontón Recoletos [10,14,15]. Torroja wrote two books [16,17] in which he explained several of his works and structural philosophy.

1.2. Structural concepts of aqueducts

Aqueducts transport water at an elevated height across some obstacle, like a valley, and resist two primary loads: the self-weight and the hydrostatic pressure exerted by the water. Those with a structural concept that avoids bending action in their walls are usually the most material-efficient.

The most efficient concept for spanning between two supports for uniformly distributed load is a parabola, for self-weight a catenary, and for hydrostatic pressure a 'hydrostatic catenary', which is Euler's elastica [18–20]. Constructing such a curve as a compressed arch is less efficient than as a tensioned chain since some bending capacity is required for the arch not to buckle.

Linear extrusion of such an arch or chain results in a cylindrical vault or channel, respectively, and if supported along their longitudinal edges, they behave like a cylindrical membrane shell with negligible longitudinal load transfer. Therefore, their structural behaviour can be approximated by that of the corresponding arch or chain. This is the case for the Brooks Aqueduct in Canada commissioned in 1914 and in operation until 1979 [21]. It has a reinforced concrete cross-section in the shape of a hydrostatic catenary, hung between firm supports, vertically consisting of longitudinal beams supported on equally spaced columns and horizontally by transverse struts. When filled with water, the load was transferred only by tensile hoop stresses, whereas with all other water levels, additional bending stresses about the longitudinal axis were present [22].

Without the longitudinal support, the structural behaviour of the channel changes substantially, requiring a capacity for longitudinal load transfer within the channel, resulting in a need for concentrated forces acting longitudinally at the top of the channel cross-section [23, pp. 460–1]. The character of the force is dependent on the support conditions. Torroja discusses in *Philosophy of structures* [16] a 'simply supported' cylindrical roof and the need for a tensile longitudinal force, see Fig. 1. Turning the roof upside down, it forms a 'simply supported' channel with a need for a compressive longitudinal force. In a 'balanced cantilevering' channel, the needed longitudinal force is tensile, and for other support conditions, it may switch signs along with the length. When the force is tensile, it may be induced by prestressing, for example, using post-tensioned high-strength steel wires. Failing to provide the needed force requires either a flexible section that adapts its geometry to accommodate a state of pure membrane stresses or additional bending stresses to complete static equilibrium, which results in reduced material efficiency.

1.3. The Alloz aqueduct

Following the completion of the Tempul aqueduct in 1925 [24,25], Torroja's office designed the 11.5 km long Alloz canal system to transport water from a reservoir near Alloz to a hydroelectric power plant near Mañeru in the Navarre province in northeast Spain. Completed

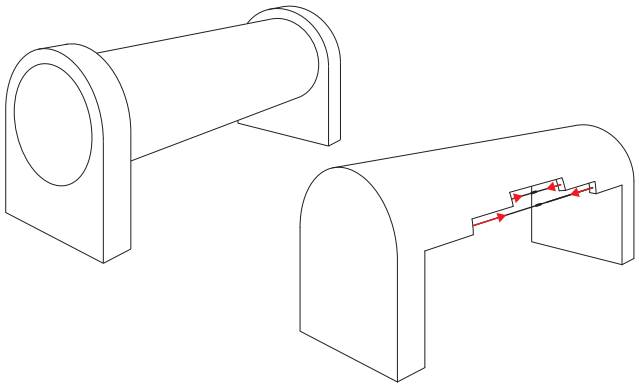

Fig. 1. A pipe between two-supports (left) and the upper half of a pipe where the need for longitudinal prestressing compensating for the missing lower half is indicated (right).
Source: Adopted from Torroja's *Philosophy of structures* [16].

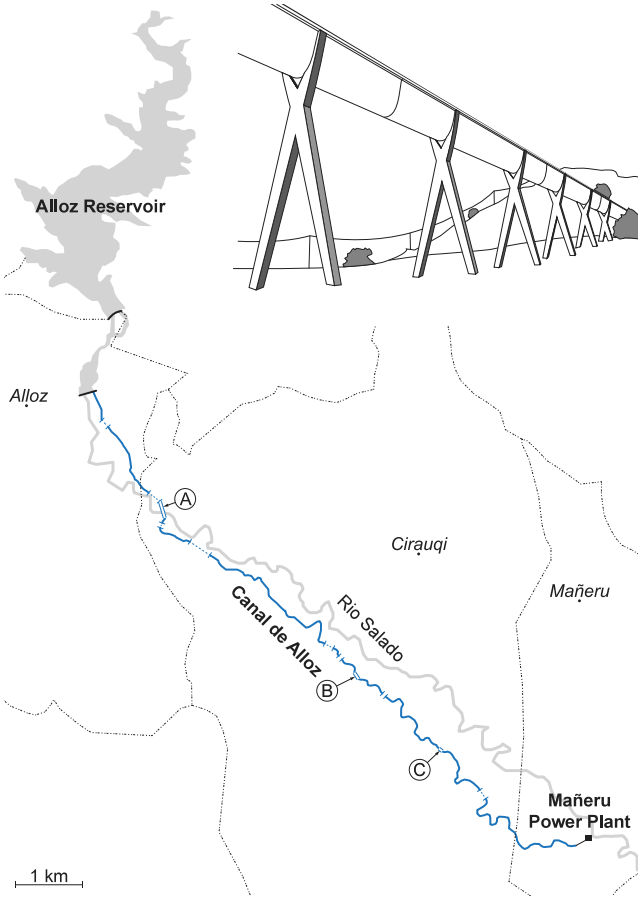

Fig. 2. Locations of aqueducts along the Alloz canal between the Alloz reservoir and the Mañeru power plant: (A) aqueduct over the Salado river, (B) across the Tejeria ravine, and (C) across the Morondoba ravine.

in 1939, the same year as the Spanish Civil War ended (1936–1939), the system consists of earth-walled channels, tunnels, and aqueducts and is still in use. There are three aqueducts, all of the same structural type [26], and the name 'Alloz aqueduct' usually refers to the longest one spanning 218 m across the Salado river, see Fig. 2. Although much more slender, the aqueducts have similarities with Alfonso Peña Boeuf's Tardienta aqueduct [27] built between 1928–1941.

The aqueducts consist of a straight U-shaped 150 mm thick concrete channel resting on X-shaped columns located every 19 m [28,29]. The

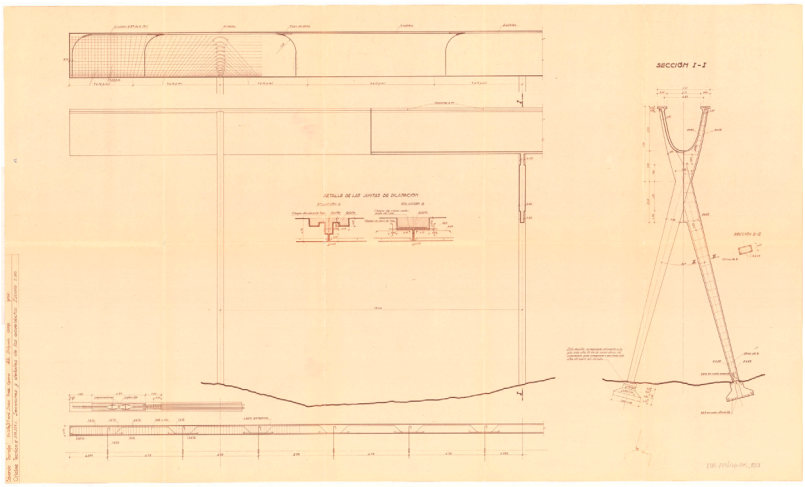

Fig. 3. Drawing containing of typical sections, elevations, and details of the Alloz aqueducts by Eduardo Torroja Oficina Técinca. *Source:* Courtesy of Archivo Torroja – CEHOPU [28].

geometry of the U-section is given by 'a third-degree parabola' [17, p. 65] whose expression can be deduced from drawings of the aqueduct [30] as $z = c|y|^3$ with $c = 2.68/1.335^3$. There are joints in the centre of every other span, so each module consists of a 19 m long central span and two 9.5 m long cantilevering spans. The arrangement ensures there is no theoretical bending moment at the middle of each span but an absolute maximum above the supports [31]. The bending moment is negative, thus the top of the cross-section is in longitudinal tension whereas the bottom is in compression.

Post-tensioned steel cables in the flanges at the upper side of the channel counteract the resulting longitudinal tensile stresses, see Fig. 3. In each flange, there are four cables over each support and two elsewhere [32]. The cables, which have hooks at the ends and are 39 mm in diameter [30], were during construction embedded in the concrete channel at the ends and elsewhere laid loosely in pairs in groves on top of the flanges. Tubes placed where the cables transition from the concrete section to the groves prevented possible cracking as the cables were stretched. Pairs of cables are held together by two clamps and, one month after casting the channel, the cables were separated at midpoint using hydraulic jacks. A bar was placed between the cables to keep the spacing after removing the jacks. The process was repeated as many times as necessary until reaching the desired stress in the cables, whereafter they were sealed into the channel by pouring concrete. The cables were post-tensioned to such an extent that the entire concrete cross-section is put in longitudinal compression. As a result, small transverse stresses appear in the section [32].

Besides containing the cables, the flanges stiffens the edges of the channel and doubles as a service footbridge. Furthermore, transverse bars with turnbuckles every 4.75 m pull the flanges together, setting the inside of the channel in compression. The accumulative effect of the longitudinal and transverse prestress renders the channel crack-free and watertight, which, according to Torroja, was 'the fundamental idea in the design of this aqueduct' [17, p. 59].

2. Theory

At least five theoretical approaches and versions thereof applicable for the design of a structure such as the Alloz aqueduct were established by the mid-1930s, including:

1. 3D elasticity theory
2. Bending theory of shells
    (a) Finsterwalder simplified bending theory for segmented circular cylindrical shells
3. Membrane theory of shells
4. Beam theory
    (a) Euler–Bernoulli beam theory
    (b) Cosserat and Timoshenko–Ehrenfest beam theories taking into account shear deformation
    (c) Griffith–Taylor theory for the bending of cantilevers
5. Plasticity theory

3D elasticity theory result in complex mathematics and practical applications lingered until numerical computer methods became readily available.

The same applies to the bending theory of shells. Although the Finsterwalder theory [33] simplifies things, it still results in 'highly complex calculations' [34]. It applies to segmented circular cylindrical shells supported by beams along the longitudinal edges, conditions the Alloz aqueduct does not fulfil. However, it is possible to alter the theory for other conditions, which Torroja did for the design of the Frontón Recoletos [10].

The membrane theory of shells is based on the assumption that there are no bending stresses present, imposing requirements on the geometry of the shell, and in the case of cylindrical shells result in simple calculations. Deviations from the 'ideal shape' results in additional bending stresses that have to be estimated by other means.

Beam theories summarise the internal stresses into resultant forces and moments and apply to structures that are much longer in one direction than the other two. Kazinczy [35] conclude that 'cylindrical shells of sufficient length l in relation to their width b (i.e. $l \geqq 2b$) may be considered as beams', which is the case for the Alloz aqueduct. Depending on assumptions made, the theories lead to different levels of accuracy. The Euler–Bernoulli 'plane sections remain plane' theory is one of the simplest and most useful beam theory. The theory ignores the effects of shear deformation and rotatory inertia, leading to underestimated deformations for beams with a span-to-depth ratio of less than 10; the Alloz aqueduct has a ratio of about 7. The Timoshenko–Ehrenfest beam theory [36] accounts for these effects at the expense of increased complexity. The Griffith–Taylor theory [37] applies to a prismatic bar loaded at its tip and assumes the same longitudinal stresses as you get from Euler–Bernoulli theory, but uses a more elaborate theory to find the shear stresses in a thick-walled beam. Torroja applied the theory for the design of the Alloz aqueduct and we return to the details later on in the paper.

The theory of plasticity allows yield stresses to occur when determining the ultimate capacity of the structure, usually leading to

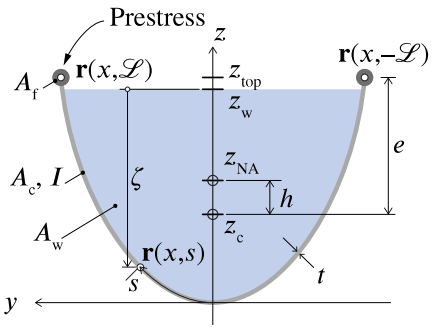

Fig. 4. Cross-section notation.

material savings compared to designs based on the theory of elasticity and can thus be used to refine initial designs based on elasticity. Contributions to its development were made in the 1930s [38], for example, by Kazinczy [39,40], who introduced the concept of plastic hinges in reinforced concrete structures [41]. It should be noted that both the membrane theory of shells and the Euler–Bernoulli theory of beams both satisfy equilibrium, and therefore if yield is not violated they both represent a lower bound and therefore safe solution.

We seek a simple conceptual understanding of the structural behaviour of the Alloz aqueduct, answering the question of whether we should think of it as a shell or a beam. Thus, we have chosen to apply and compare the membrane theory of cylindrical shells and the Euler–Bernoulli beam theory, outlined in grater detail the following.

2.1. Coordinate system

Let the directrix of the cylindrical channel be in the direction of the x-axis and let the generatrix representing the middle curve of the cross-section be a plane curve in the yz-plane. Restrict the attention to symmetric cross-sections positioned so that $z = 0$ at the bottom of the cross-section curve. Let s be the arc length parameter of the cross-section curve, measured from the bottom of the cross-section curve, and let $s = \pm\mathcal{L}$ at the top, see Fig. 4. Any point on the middle surface can then be described by the position vector

$$\mathbf{r} = (x, y(s), z(s)), \tag{1}$$

whose first and second derivatives with respect to s are the tangent vector and the curvature vector of the cross-section curve, respectively. Let λ be the slope, κ the curvature, and R the radius of curvature of the cross-section so that

$$\frac{dy}{ds} = \cos\lambda, \tag{2}$$

$$\frac{dz}{ds} = \sin\lambda, \tag{3}$$

$$\kappa = \frac{1}{R} = \frac{d\lambda}{ds}. \tag{4}$$

The middle surface of the channel may then be unrolled to a flat plane perpendicular to the z-axis with coordinates (x, s).

2.2. In-plane equilibrium and stress–strain relations

The load acting on the aqueduct is the sum of water weight and the self-weight. Therefore, the normal pressure p is given by the sum of the hydrostatic pressure and the normal component of the self-weight, the body force p_s in the hoop direction given by the component of the self-weight tangential to the surface, and the body force p_x in the longitudinal direction is zero, all measured as force per unit surface area. The self-weight and water weight are constant along the length

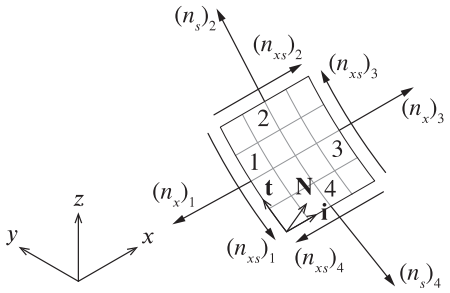

Fig. 5. Membrane stress resultants, measured as force per unit cross-section width, acting on the four sides of a small curvilinear square cylindrical shell element with side lengths δ_x and δ_s, respectively. Summing up the stresses in the s-direction gives $(n_s)_2\,\delta_x - (n_s)_4\,\delta_x + (n_{xs})_1\,\delta_s - (n_{xs})_3\,\delta_s + p_s\delta_x\delta_s = 0$ or, by dividing with the area $\delta_x\delta_s$, $[(n_s)_2 - (n_s)_4]/\delta_s + [(n_{xs})_1 - (n_{xs})_3]/\delta_x + p_s = 0$ where p_s is the component of body force per unit surface area acting in the hoop direction. If the element area is taken smaller and smaller, i.e. $\delta_x, \delta_s \to 0$, the limit of $[(n_s)_2 - (n_s)_4]/\delta_s$ becomes $\partial n_s/\partial s$ by the definition of such a derivative. Similarly $[(n_{xs})_1 - (n_{xs})_3]/\delta_x$ becomes $\partial n_{xs}/\partial x$. The equation of equilibrium is obtained in the longitudinal direction in the same manner.

of the aqueduct, so all load components are independent of x, allowing the abbreviations

$$\frac{\partial p}{\partial s} = \frac{dp}{ds} = p', \qquad \frac{\partial p_s}{\partial s} = \frac{dp_s}{ds} = p_s', \tag{5}$$

and similarly for higher-order derivatives with respect to s.

The load acting on the aqueduct give rise to membrane stresses acting in a plane tangential to the surface of the channel, see Fig. 5. For both the membrane shell theory and the Euler–Bernoulli beam theory, the membrane stress resultants are in equilibrium when

$$\left.\begin{aligned} \frac{\partial n_s}{\partial s} + \frac{\partial n_{xs}}{\partial x} + p_s = 0 \\ \frac{\partial n_{sx}}{\partial s} + \frac{\partial n_x}{\partial x} = 0 \end{aligned}\right\}, \tag{6}$$

where n_x is the longitudinal membrane stress resultant, n_s the hoop membrane stress resultant, and $n_{xs} = n_{sx}$ the shear membrane stress resultant, all measured per unit cross-section width of the middle surface. The relation between stress resultant and stress measured per unit cross-section area is for the different directions given by

$$n_x = \sigma_x t, \quad n_{xs} = \tau_{xs} t, \quad n_s = \sigma_s t. \tag{7}$$

Eq. (6) is not enough to arrive at a complete state of stress in equilibrium, and a third expression is needed. In the shell membrane theory, Eq. (6) is complemented with an equation describing the equilibrium between the internal stresses and the normal load p. In the Euler–Bernoulli beam theory, we assume the load components in the hoop direction and the normal direction to be zero ($p_s = 0$, $p = 0$). Nevertheless, the effect of these load components is still present, which we for the symmetric cross-section consider by using an equivalent uniformly distributed vertical load acting along the neutral axis of the cross-section giving rise to a beam bending moment. If the cross-section is asymmetric, an additional equivalent twisting moment is required. Assumptions about the relation between the beam bending moment and the longitudinal stress distribution result in a third expression which together with Eq. (6) describe the membrane stresses. However, these membrane stresses are, in general, not in equilibrium, giving rise to bending stress about the longitudinal axis.

We assume an isotropic elastic material, leading to constitutive stress–strain relations given by

$$\left.\begin{aligned} \epsilon_x &= \left(n_x - \nu n_s\right)/(Et) \\ \gamma_{xs} &= (1+\nu) n_{xs}/(Et) \\ \epsilon_s &= \left(n_s - \nu n_x\right)/(Et) \end{aligned}\right\}, \tag{8}$$

in which t is the wall thickness, E is the elastic modulus, and ν Poisson's ratio. Usually, the wall thickness does not appear in these relations but is needed to make the strains unitless since we here use stress resultants measured per unit cross-section width rather than stress per unit cross-section area.

2.3. Cylindrical membrane shell theory

Membrane shell theory implicitly gives the preconditions for a material-efficient structural concept that may fully utilise the material strength, which stands in contrast to those that include bending action, where full strength-utilisation only can be achieved in the outermost material fibre of the cross-section. The theory relies on a set of assumptions that requires the solution to be statically determinate.

By establishing an equilibrium in the normal direction of the channel, an expression for the hoop stress is found as

$$\hat{n}_s = Rp, \tag{9}$$

where p is the normal load measured per unit surface area. A hat $\hat{}$ is used throughout the paper to denote quantities related to the cylindrical membrane shell theory so that these are not confused with those of the Euler–Bernoulli beam theory, denoted with a ring $\mathring{}$.

With $\hat{n}_s$ given by Eq. (9) inserted in the first expression in Eq. (6) and using the resulting expression for $\hat{n}_{xs}$ inserted in the second expression of Eq. (6), the complete state of membrane stress for the aqueduct channel is obtained as

$$\left.\begin{aligned} \hat{n}_x &= \frac{x^2}{2}\left(\hat{n}_s'' + p_s'\right) + xC_1'' + C_2'' \\ \hat{n}_{xs} &= -\left(x\left(\hat{n}_s' + p_s\right) + C_1'\right) \\ \hat{n}_s &= Rp \end{aligned}\right\}, \tag{10}$$

where C_1 and C_2 are two statically indeterminate scalar functions in s.

With u, v, and w the assumed small displacements in the longitudinal, hoop, and normal directions, respectively, of the cylindrical shell, the kinematic relations between strains and displacements are given by

$$\left.\begin{aligned} \epsilon_x &= \frac{\partial u}{\partial x} \\ \gamma_{xs} &= \frac{1}{2}\left(\frac{\partial u}{\partial s} + \frac{\partial v}{\partial x}\right) \\ \epsilon_s &= \frac{\partial v}{\partial s} + \frac{w}{R} \end{aligned}\right\}. \tag{11}$$

By combining Eqs. (8) and (11) and integrating once where needed, explicit expressions for the displacements are obtained. With constant wall thickness t, which is the case for the Alloz aqueduct, the displacement field is given by

$$\left.\begin{aligned} u &= \frac{1}{Et}\int^x \left(\hat{n}_x - \nu\hat{n}_s\right)\,dx + \frac{C_3}{Et} \\ v &= \int^x \left(\frac{2(1+\nu)}{Et}\hat{n}_{xs} - \frac{\partial u}{\partial s}\right)dx + \frac{C_4}{Et} \\ w &= R\left(\frac{1}{Et}\left(\hat{n}_s - \nu\hat{n}_x\right) - \frac{\partial v}{\partial s}\right) \end{aligned}\right\}, \tag{12}$$

where C_3 and C_4 are functions in s.

2.3.1. Boundary conditions and the need for prestress

For cylindrical shells with continuous vertical supports along the longitudinal edges, the shear stress and longitudinal stress must be independent of x, thus zero or constant. Then, with flexible walls in bending and assuming that the water weight is much larger than the self-weight, the aqueduct must have the shape of a so-called 'hydrostatic catenary', which curvature is proportional to the distance from the water surface. The hydrostatic catenary is the same curve as Euler's Elastica [18–20], which curvature is proportional to the distance from the line of action of the force. An example of an aqueduct with such a cross-section curve is the Brooks Aqueduct in Canada, which was commissioned in 1914 and in operation until 1979 [21,22]. When filled with water, the load was carried only by tensile hoop stresses in the reinforced concrete section, whereas with all other water levels, additional bending stresses about the longitudinal axis were present in the shell.

The Alloz aqueduct does not have continuous but intermediate vertical supports along the longitudinal edges of the channel. For such cases, the shear stress and longitudinal stress must change with x. Then, to satisfy the equilibrium along the longitudinal edges, there must be a prestress tension $T(x)$ along the top of each side of the cross-section [23, pp. 460–1] such that

$$\hat{n}_{xs} = \pm\left(-\frac{dT}{dx}\right) \text{ when } s = \pm\mathcal{L}. \tag{13}$$

Hence, Eq. (13) tells us that the material-efficient structural concept of a cylindrical membrane shell is connected to the use of prestressing.

2.3.2. Self-weight and water loading

Loaded with self-weight and with water, the normal load is given by

$$p = p_c + p_w, \tag{14}$$

$$p_c = \rho_c g t\cos\lambda, \tag{15}$$

$$p_w = \rho_w g\zeta, \tag{16}$$

$$\zeta = \max\left(z_w - z, 0\right), \tag{17}$$

where ρ_c is the density of the concrete wall, ρ_w the density of the water, g the standard acceleration due to gravity, ζ the non-negative depth of the water, and z_w the top of the water. Assume no 'support from above', that is, no support along the edges of the shell where $s = \pm\mathcal{L}$, then

$$n_s = 0 \quad \text{when } s = \pm\mathcal{L}. \tag{18}$$

The hoop stress $\hat{n}_s$ of Eq. (10) combined with Eqs. (14)–(18) then tells us that the wall should be vertical ($\cos\lambda = 0$) between the top level of the water, z_w, and the top of the shell, $z_{top} = z(\mathcal{L})$, to carry its self-weight, just as the Shahe Aqueduct in China, although this could perhaps be relaxed if some bending is allowed. But certainly, the condition in Eq. (18) means that the structure will be flexible in the normal direction along the top edges and should therefore be provided with a stiffening lip or horizontal beam, just as the Alloz aqueducts have.

2.3.3. Influence of the cross-section

The stresses in Eq. (10) are proportional to the radius of curvature R of the cross-section curve, which is the inverse of the curvature κ. For an arbitrary plane cross-section curve given by $z = f(y)$, the curvature is given by

$$\kappa = \frac{f''(y)}{\left(1 + f'(y)^2\right)^{3/2}}. \tag{19}$$

where $f'(y)$ is used to denote derivatives with respect to y and similar for higher-order derivatives.

The Alloz aqueduct have a cross-section given by a cubic parabola $z = f(y) = c|y|^3$. Hence, the curvature is

$$\kappa = \frac{6cy^2}{|y|\left(1 + 9c^2y^4\right)^{3/2}}, \tag{20}$$

which tend to zero as $y, s \to 0$. Therefor, the radius of curvature tend to infinity as $y, s \to 0$. As a consequence, Eq. (10) tells us that for a cubic parabola there will be infinite hoop stress along the centre line $s = 0$. In reality, if the wall is flexible enough in bending, the cross-section will change its geometry to relax such a stress concentration.

2.4. Euler–Bernoulli beam theory

The formulas of this section are based on the Euler–Bernoulli beam theory and take into account the effect of combining concrete and reinforcement steel, something Kazinczy reported on in 1933 [39]. In 1949, he applied these principles for the design of cylindrical reinforced concrete shells [35] in a similar manner as we have proposed in the following.

Assume the wall thickness t to be thin but variable and that longitudinal strains can be calculated using plane sections remain plane and perpendicular to the longitudinal axis, as is assumed in Euler–Bernoulli beam theory [42]. Then, with notations indicated in Fig. 4, the longitudinal bending strains are equal to the distance below the elastic centroid, z_c, multiplied by the sagging curvature.

2.4.1. Prestress and equivalent cross-section

With the simultaneous presence of a beam bending moment, $M = M(x)$, and a longitudinal prestress force, $P = P(x)$, shared between the two sides induced at an eccentricity e above the cross-section centroid z_c by means of tension wires, the total sagging moment is

$$M_{\text{total}} = M + Pe. \tag{21}$$

If the moment M is hogging, as is the case for the Alloz aqueduct, Pe will reduce the absolute value of the moment. Regardless, the longitudinal tensile membrane stress is given by

$$\mathring{n}_x = \frac{(M+Pe)}{I} t\left(z_c - z\right) - \frac{Pt}{A_c}, \tag{22}$$

where A_c and I are the cross-sectional area and second moment of area of the solid concrete wall. A ring $\mathring{}$ is used throughout the paper to denote quantities related to the Euler–Bernoulli beam theory so that these are not confused with those of the cylindrical membrane shell theory, denoted with a hat $\hat{}$.

With varying thickness t, the cross-sectional properties are given by

$$A_c = 2\int_{\eta=0}^{\mathcal{L}} t(\eta)\, d\eta, \tag{23}$$

$$z_c = \frac{2}{A_c}\int_{\eta=0}^{\mathcal{L}} t(\eta) z(\eta)\, d\eta, \tag{24}$$

$$I = 2\int_{\eta=0}^{\mathcal{L}} t(\eta)\left(z_c - z(\eta)\right)^2 d\eta, \tag{25}$$

which are constants and do neither vary in the longitudinal nor the hoop direction.

The prestress may be considered as an applied load with no accompanying elastic stiffness. Assume the prestress arranged to be proportional to the hogging moment due to vertical loading so that

$$Pe = -\mu M, \tag{26}$$

where μ is a dimensionless constant and the minus sign is to make Pe positive when M is sagging. Then

$$\mathring{n}_x = \frac{M}{\tilde{I}} t(s)\left(z_{\text{NA}} - z(s)\right), \tag{27}$$

where the modified second moment of area $\tilde{I}$ and the level of the modified centroid, which coincide with the level of the neutral axis z_{NA}, are

$$\tilde{I} = \frac{I}{1-\mu}, \tag{28}$$

$$z_{\text{NA}} = \tilde{I}\left(\frac{1-\mu}{I} z_c + \frac{\mu}{eA_c}\right) = z_c + h. \tag{29}$$

Note that $\mu = 1$ makes perfect physical sense because then there is no bending of the section and it is in a state of uniform compression with the neutral axis at infinity ($z_{\text{NA}} = \infty$). If $\mu > 1$, then $\tilde{I}$ is negative, which means that the prestress and eccentricity are sufficient to reverse the curvature due to vertical loading.

The prestress force could, instead of using tension wires, be generated by the addition of a concentrated area A_f, shared between the two sides, and a simple elastic stiffness, such that

$$\left(A_c + A_f\right) z_{\text{NA}} = A_c z_c + A_f\left(z_c + e\right), \tag{30}$$

$$A_f = \frac{h}{e-h} A_c. \tag{31}$$

As one would expect, an infinite area A_f would be required to move the centroid so that $h = e$.

2.4.2. Membrane stress state

With $\mathring{n}_x$ given by Eq. (27), the membrane stresses in the cross-section are given using Eq. (6) by setting $p_s = 0$ and $p = 0$ since the effect on the membrane stresses of these load components is accounted for already when determining the beam bending moment M influencing $\mathring{n}_x$. Thus, with $\mathring{n}_x$ inserted in the second expression in Eq. (6) and using the resulting expression for $\mathring{n}_{xs}$ inserted in the first expression of Eq. (6), the complete state of membrane stress is obtained as

$$\left.\begin{aligned} \mathring{n}_x &= \frac{M}{\tilde{I}} t(s)\left(z_{\text{NA}} - z(s)\right) \\ \mathring{n}_{xs} &= -\frac{d}{dx}\left(\frac{M}{\tilde{I}} B(s) + F_1\right) \\ \mathring{n}_s &= \frac{d^2}{dx^2}\left(\frac{M}{\tilde{I}}\int_{\eta=0}^{s} B(\eta)\, d\eta + sF_1\right) - \frac{dF_2}{dx} \end{aligned}\right\}, \tag{32}$$

where F_1 and F_2 are two statically indeterminate scalar functions in x and

$$B(s) = \int_{\eta=0}^{s} t(\eta)\left(z_{\text{NA}} - z(\eta)\right)\, d\eta, \tag{33}$$

is the first moment area of the cross-section from the centre-line to s about the neutral axis.

Due to symmetry, the shear stress must be zero along the middle line ($s = 0$). Inserting $s = 0$ into Eq. (33) gives $B(0) = 0$ and, from the second expression in Eq. (32), follows

$$\frac{dF_1}{dx} = 0. \tag{34}$$

If we assume no 'supports from above', then $n_s = 0$ for $s = \pm\mathcal{L}$. Note that $\int_0^s B(\eta)\, d\eta = \int_0^{-s} B(\eta)\, d\eta$ due to symmetry, thus, from the third expression in Eq. (32), follows

$$\frac{dF_2}{dx} = \frac{d^2M}{dx^2}\frac{1}{\tilde{I}}\int_{\eta=0}^{\mathcal{L}} B(\eta)\, d\eta. \tag{35}$$

With dF_1/dx and dF_2/dx known, the stress state in Eq. (32) reduces to

$$\left.\begin{aligned} \mathring{n}_x &= \frac{M}{\tilde{I}} t(s)\left(z_{\text{NA}} - z(s)\right) \\ \mathring{n}_{xs} &= -\frac{dM}{dx}\frac{1}{\tilde{I}} B(s) \\ \mathring{n}_s &= \frac{d^2M}{dx^2}\frac{1}{\tilde{I}}\left(\int_{\eta=0}^{s} B(\eta)\, d\eta - \int_{\eta=0}^{\mathcal{L}} B(\eta)\, d\eta\right) \\ &= -\frac{d^2M}{dx^2}\frac{1}{\tilde{I}}\int_{\eta=s}^{\mathcal{L}} B(\eta)\, d\eta. \end{aligned}\right\}. \tag{36}$$

2.4.3. Wall bending moment

In pure membrane theory, the shape described by the curvature κ is such that the stresses equilibrate the applied load, resulting in a membrane stress state given by Eq. (10). If the point of departure instead is the Euler–Bernoulli beam theory, Eq. (36) describes the corresponding membrane stress state. If the cross-section shape is such that it does not act as a pure membrane, additional wall bending moments about the longitudinal axis arises

$$m = m_w + m_c + m_\tau. \tag{37}$$

Fig. 6 illustrates the forces $p_w d\eta$, $p_c d\eta$, and $n_s' d\eta$ acting on the small segment $d\eta$ that contributes m_w, m_c, and m_τ, respectively, given by

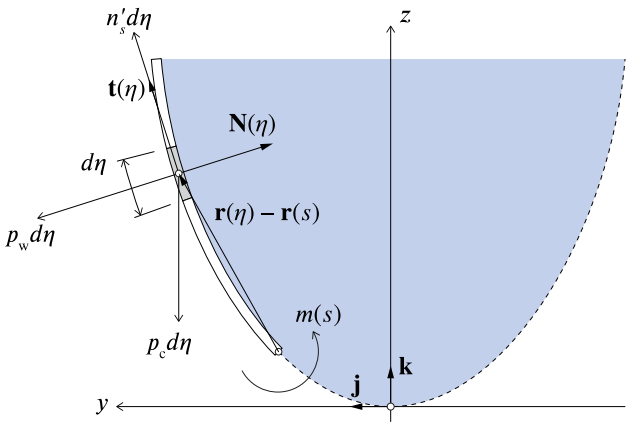

Fig. 6. Applied forces on a short wall segment $d\eta$ positioned at $\mathbf{r}(\eta)$ contributing to the wall bending moment m about a point $\mathbf{r}(s)$ on the cross-section.

taking moments about $\mathbf{r}(s)$ and integrating from the point $\mathbf{r}(s)$ to the top of the cross-section $\mathbf{r}(\mathcal{L})$.

The contributions to the moment from hydrostatic pressure and the self-weight are

$$m_w = \int_{\eta=s}^{\mathcal{L}} p_w \left(\mathbf{r}(\eta) - \mathbf{r}(s)\right) \times \mathbf{N}(\eta)\, d\eta \cdot \mathbf{i}, \tag{38}$$

$$m_c = \int_{\eta=s}^{\mathcal{L}} p_c \left(\mathbf{r}(\eta) - \mathbf{r}(s)\right) \times \mathbf{k}\, d\eta \cdot \mathbf{i}, \tag{39}$$

where $\mathbf{i}$ and $\mathbf{k}$ are the Cartesian base vectors in the x and z direction, respectively, and $\mathbf{N} = R\partial^2\mathbf{r}/\partial s^2$ the surface inwards unit normal vector.

The force $n_s' d\eta$ is equal to the difference in shear stress acting on two parallel cross-sections positioned at a small distance from one another, and if this small distance is taken to the limit

$$n_s' d\eta = \frac{\partial n_{xs}}{\partial x} d\eta, \tag{40}$$

meaning the rate of change in hoop stress n_s' is driven by the rate of change of shear stress in the longitudinal direction. Therefore, we refer to this wall bending moment contribution as a 'shear stress contribution' denoted with a subscript τ. The contribution is given by

$$\begin{aligned} m_\tau &= \int_{\eta=s}^{\mathcal{L}} \mathring{n}_s' \left(\mathbf{r}(\eta) - \mathbf{r}(s)\right) \times \mathbf{t}(\eta)\, d\eta \cdot \mathbf{i} \\ &= -\int_{\eta=s}^{\mathcal{L}} \kappa \mathring{n}_s \left(\mathbf{r}(\eta) - \mathbf{r}(s)\right) \times \mathbf{N}(\eta)\, d\eta \cdot \mathbf{i}, \end{aligned} \tag{41}$$

where $\mathbf{t} = \partial\mathbf{r}/\partial s$ is the surface unit tangent vector in the hoop direction. The last equality in Eq. (41) follow from integration by parts where we make use of the fact that $\mathring{n}_s(\mathcal{L}) = 0$ and $\mathbf{t}' = \partial^2\mathbf{r}/\partial s^2 = \kappa\mathbf{N}$.

Again, the Alloz aqueducts have a cross-section curve given by a cubic parabola with curvature given by Eq. (20) tending to 0 as $y, s \to 0$. As a consequence, the shear contribution m_τ to the bending moment m will be rather low around $s = 0$ compared to other choices of cross-sections such as a circle (κ = constant), a parabola ($\kappa(0) = \kappa_{\max}$), or catenary ($\kappa(0) = \kappa_{\max}$). Since m_τ reduces m, the cubic parabola is expected to have a relatively high bending moment along $s = 0$.

3. Does it act as a shell or a beam?

Both the Euler–Bernoulli beam theory and the membrane theory of cylindrical shells were available at the time and could have been used to design the Alloz aqueduct. However, neither of them provide a complete description of the aqueduct's structural behaviour. The Euler–Bernoulli beam theory gives a proper overall stress distribution in the longitudinal direction but does not guide the choice of an efficient cross-section shape, while the membrane theory of cylindrical shells does the opposite. Furthermore, the latter requires prestressing along the longitudinal edges to provide solutions in equilibrium. To better understand Torroja's considerations and calculations, we apply and compare these two theoretical approaches, roughly asking which theory best describes the behaviour.

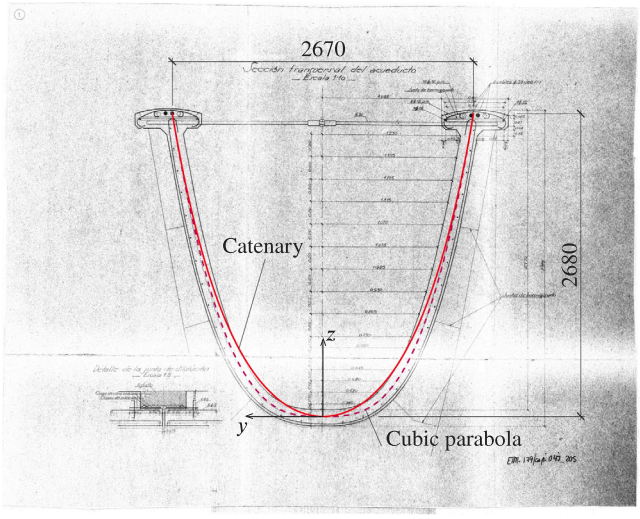

Fig. 7. Section drawing of the Alloz aqueduct with cubic parabola and catenary overlay.
Source: Drawing courtesy of Archivo Torroja – CEHOPU [30].

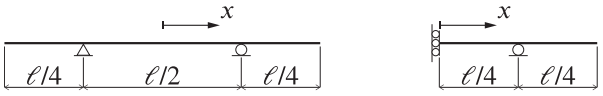

Fig. 8. Boundary conditions for the complete aqueduct (left) and the considered part (right).

We consider an aqueduct of total length $\ell = 38$ m with similar boundary conditions as the Alloz aqueduct. The cubic parabola shaped cross-section of the Alloz aqueduct has zero curvature at the bottom, so using it leads to infinite hoop stress and, therefore, infinite deformation along the centre line according to the membrane theory of shells. To avoid this, we use a cross-section of constant thickness $t = 0.15$ m in the shape of a catenary given by

$$\left.\begin{aligned} y(s) &= c \sinh^{-1}\frac{s}{c} \\ z(s) &= c\sqrt{\frac{s^2}{c^2} + 1} - c \end{aligned}\right\}. \tag{42}$$

With $y(\pm\mathcal{L}) = \pm 1.335$ m and $z(\pm\mathcal{L}) = 2.68$ m, the constant $c \approx 0.5402$, resulting in a cross-section with only a slight deviation in geometry compared to the true cross-section, see Fig. 7.

With the coordinate system positioned so that $x = 0$ is halfway along the aqueduct and due to symmetry in both geometry and loading, only one half needs to be considered, see Fig. 8. For the membrane shell theory, Appendix A.1 provides expressions for the displacement and functions C_1–C_4 for the considered boundary conditions. Similarly, for the beam theory, Appendix A.2 provides expressions for the beam bending moment and the deflection.

We consider three load cases: only water weight (LC1); only self-weight (LC2), and; both self-weight and water weight (LC3). The density of the water is taken as $\rho_c = 1{,}000$ kg/m^3 and of the concrete wall as $\rho_c = 2{,}400$ kg/m^3.

Most expressions are analytical and exact, and only a few integrals and optimisation problems related to finding the μ values require numerical solution approaches. Using Wolfram Mathematica 11.3 running on a Windows 10 laptop equipped with an Intel Xeon CPU @ 2.80 GHz, it takes about 10 s to compute the results for each load case.

Table 1
Prestress force $P_{\max}$ (MN) at the support location ($x = \ell/4$) according to the Euler–Bernoulli beam theory and corresponding compressive stress in the concrete flange σ_{flange} (MPa) and levels of prestress μ.

Prestress level		P_σ	P_τ	P_{m}	Torroja
$P_{\max}$		1.69	16.41	19.08	1.84
σ_{flange}		11.7	114.0	132.5	12.9
μ	LC1	1.11	10.73	12.48	–
	LC2	2.50	24.27	28.21	
	LC3	0.77	7.44	8.65	

3.1. Prestress force

Combining Eqs. (26) and (51) gives an explicit expression for the compressive prestress force P shared between the two flanges in which the prestressing cables are embedded. P will have its maximum value $P_{\max}$ above the support ($x = \ell/4$).

For the beam theory, we consider four values for the prestress force, enabling the exploration of the influence of the longitudinal prestressing: no prestress ($P = 0$); prestress so that the longitudinal stress at the top of the section ($s = \pm\mathcal{L}$) is zero in the flanges ($P = P_\sigma$); prestress so that the beam shear stress at the top of the section is equal to the shell shear stress ($P = P_\tau$), and; prestress so that the wall bending moment is minimised at $s = 0$ ($P = P_{\text{m}}$). The prestress forces are computed considering LC3 combining Eqs. (26) and (51), and Table 1 show the maximum prestress force and corresponding μ values for the different load cases.

Assuming the dimensions of each flange to be 600×120 mm (see Fig. 3), the force $P_{\max}$ results in viable levels of stress in the concrete, σ_{flange}, for P_σ, whereas for P_τ and P_{m}, it is far beyond the compressive strength of most concrete qualities available in 1939, see Table 1.

3.2. Membrane stresses

Fig. 9 display the hoop stress σ_s, shear stress τ_{xs}, and longitudinal stress σ_x at the support location ($x = \ell/4$) for LC1–LC3 computed using the membrane shell theory and the beam theory. The stress plots have the same shape and proportions for any cut, only the magnitude of the stresses will differ.

For LC1, the hoop stress σ_s is zero in the flanges at the top of the cross-section regardless of theory and prestress level, whereas for LC2 and LC3, the shell theory results in tensile hoop stress at the top of the section (Fig. 9, top).

Without any prestress ($P = 0$), the stress levels of the beam theory are relatively low compared to those of the shell theory. Furthermore, the longitudinal stress σ_x in the beam is such that the top of the cross-section is in tension while the central part is in compression, whereas for the shell theory, the central part is always in tension (Fig. 9, bottom).

By increasing the prestressing so that the longitudinal stress is zero along with the flanges ($P = P_\sigma$), the entire beam cross-section becomes longitudinally compressed. The compression reduces the risk of cracks on the inside, as was the design intent with the Alloz aqueduct.

Increasing the prestress to $P = P_\tau$ makes the shear stress at the top of the cross-section according to the beam theory match the shear stress of the shell theory. Then, in LC1 and LC3, the stress state of the beam theory almost matches that of the shell theory. The beam is then prestressed to such a degree that it acts almost like a membrane shell. However, the longitudinal stress will then be a mix of tensile and compressive stresses with risks of cracks on the inside.

3.3. Wall bending moment

Fig. 10 display the wall bending moment complementing the membrane equilibrium of the cross-section wall using the beam theory. The bending moment decreases with an increased level of prestress. In fact, it is possible to find a level of prestress $P = P_{\text{m}}$ such that $m = 0$ at $s = 0$, resulting in minor bending moments at the position of the shear maximum points (see Fig. 9). The beam is then prestressed to such a degree that its load-carrying action resembles a membrane shell, again highlighting the need for prestressed longitudinal edges for the cylindrical shell membrane theory. If a circular cross-section would have been used, finding P_{m} such that $m = 0$ at $s = 0$ would give $m = 0$ for any s.

The bending-moment capacity of a wall similar to the Alloz aqueduct channel wall is about 41.6 kNm/m (assume: 150 mm thick concrete with Young's modulus 30 GPa, Poisson's ratio 0.15, compressive strength 25 MPa; $9\phi15$ reinforcement bars per metre with yield strength 250 MPa placed on the tension side with 30 mm concrete cover). Hence, in accordance with the lower-bound theorem [2] and even without any prestress ($P = 0$), the wall has the capacity to resist the bending moment that arises.

For prestress levels $P \leq P_m$, the bending moment is positive meaning that the inside of the wall is in tension whereas the outside is in compression. This imposes a risk for cracks on the water side with accelerated corrosion of the reinforcement steel and water leakage. To overcome this risk, Torroja imposed a larger negative bending moment on the Alloz aqueduct wall by means of transverse ties with turn buckles that pulls the flanges together, effectively putting the inside in compression and the outside in tension. For a prestress level of P_σ, the bending moment is 30.33 kNm/m. With transverse ties placed every 4.75 m, the magnitude of the force in each needed to make the bending moment negative is about 54 kN.

3.4. Deformations

Fig. 11 display the vertical displacement of the neutral axis of the aqueduct computed using the beam theory. Without prestress, the tip of the cantilever sags for any load case, whereas with prestress P_σ, the tip sags only a little for LC3 and rises for LC1 and LC2, but the overall deformation is insignificant regardless of load case. With prestress P_τ and P_{m}, the tip rises with magnitudes comparable to the displacement obtained for the upper part of the cross section using the shell theory, see Fig. 12, although such displacements are unreasonably high from a serviceability perspective.

Fig. 12 display the deformed channel according to membrane theory of shells for LC1. The longitudinal edges move substantially inwards with increased distance from the support ($x = \ell/4$) with a maximum value of about 100 mm, again highlighting the importance of providing the shell with a stiffening lip at the top of the cross-section. At the bottom of the tip of the cantilever, the shell deforms downwards about 116 mm (for LC3, 145 mm downwards), forming a sharp kink that could possible damage the sealing between one aqueduct module and the next. The deformation of the bottom part of the wall can be reduced if the wall is provided with some bending stiffness. Furthermore, at the top of the tip of the cantilever, the shell deforms upwards due to the prestress needed to complete the equilibrium of the longitudinal edges.

4. Torroja's design approach

Torroja described the Alloz aqueduct in his books [16,17] and papers [31,32,43], but none of these contain detailed information of the analysis undertaken during the design. However, among the extensive collection of original drawings (see e.g. Figs. 3 and 7), sketches, and documents in the Archivo Torroja are two documents of particular interest: *Teoría del método de la lámina de jabón* (Theory of the soap-film

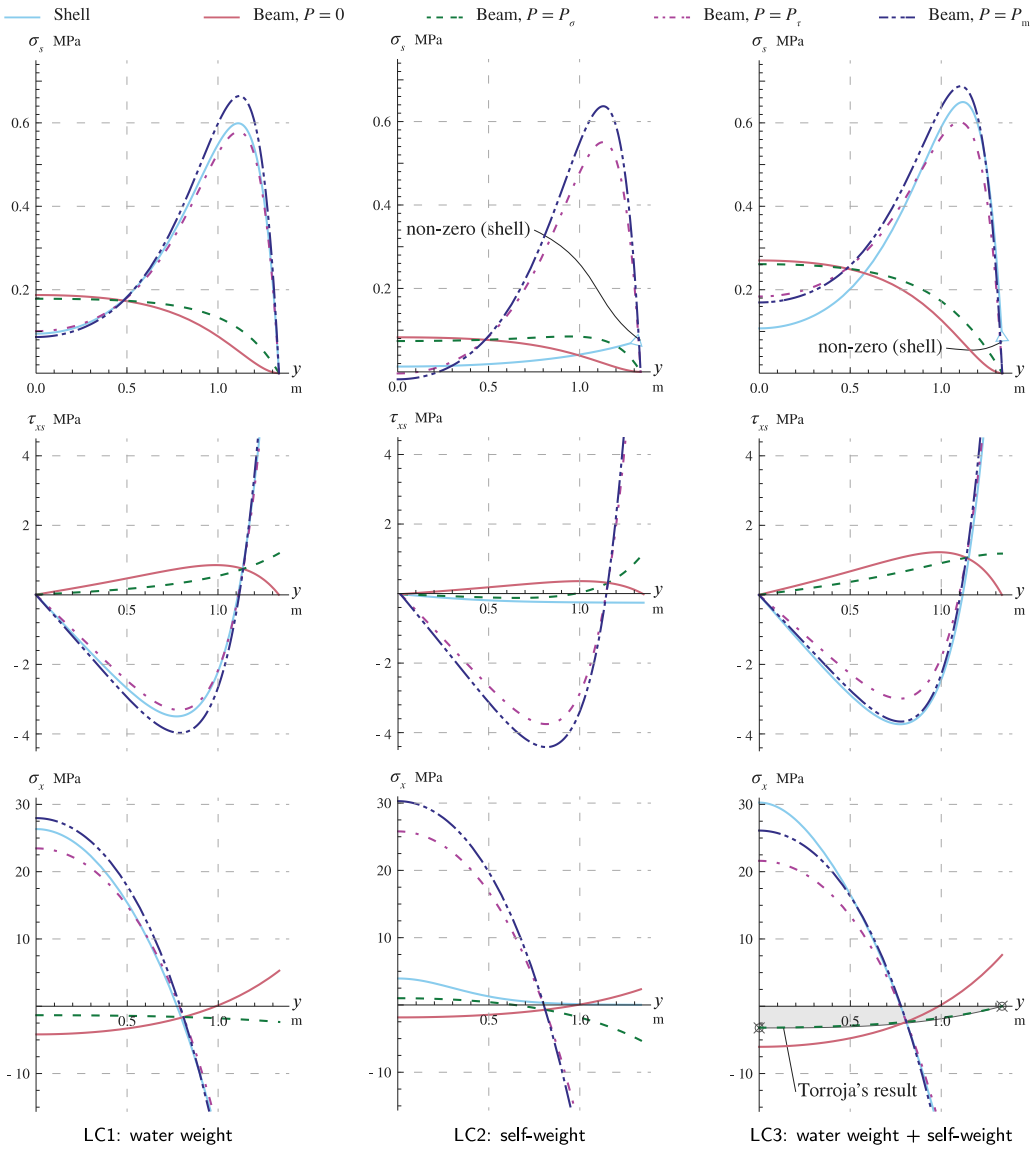

Fig. 9. Membrane stresses in catenary shaped channel at the support location ($x = \ell/4$) for load cases LC1–LC3 according to membrane theory of shells and Euler–Bernoulli beam theory. Prestress forces for the beam theory: no prestress ($P = 0$), prestress making the hoop stress zero in the flanges at $s = \pm\mathcal{L}$ ($P = P_\sigma$), prestress making the shear stress of the two theories match at $s = \pm\mathcal{L}$ ($P = P_\tau$), and prestress minimising the wall bending moment at $s = 0$ ($P = P_m$), all determined considering LC3.

method) from 1939 [44] and *Calculo del acueducto de Alloz* (Calculation of the Alloz aqueduct) from 1940 [45]. Unfortunately, the author(s) and the status of these documents are unknown, and they contain typos, especially in the equations, leaving room for interpretation and uncertainties. The documents do not contain any discussion on displacements of the aqueduct or long-term losses in prestress forces and concrete stiffness, at that time little known issues. However, we believe the documents reveal enough to conclude how Torroja design the Alloz aqueduct.

4.1. Theory

The theory document [44] is an extract from another document, *'Instruccion E. 20,1'*, not found in the archive, presumably containing the theoretical background to the used expressions. However, upon translating to English, the writings appear partly the same as in Articles 105 *Bending of a Cantilever* and 113. *The Solution of Bending Problems by the Soap-film Method* in *Theory of Elasticity* by Timoshenko and Goodier from 1951 [46], first published by just Timoshenko in 1934, six years before the completion of the Alloz aqueduct.

Article 105 introduces general assumptions on the nature of the bending problem of cantilevering prismatical bars loaded at their tip. Article 113 reports theory presented by Griffith and Taylor in 1917 [37] that make use of a soap-film analogy to establish a stress function in the plane of the cross-section to find the components of shear stress in a beam which does not have thin walls, and so the usual consideration of shear flow in the Euler–Bernoulli theory fails. The theory draws upon Prandtl's soap-film analogy for torsional problems [46, Art. 93]. In essence, the Griffith–Taylor theory for the bending of cantilevers is an elaboration of the Euler–Bernoulli beam theory, and we are uncertain as to why Torroja decided to use the theory when he just as well could have used the simpler beam theory for a relatively thin-walled structure.

With x the vertical downwards axis, y the horizontal, and z the longitudinal axis, all acting through the centre of gravity of the cross-section, the following summarise the theory:

1. Assume that a cantilevering prismatic bar of length ℓ and with second moment of area I loaded with downwards acting load P at its tip sufficiently describe the structural behaviour.

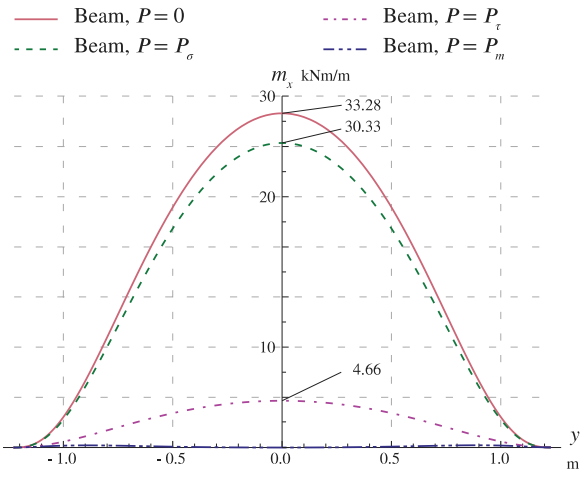

Fig. 10. Wall bending moment m for catenary shaped channel for LC3 (water weight + self-weight) according to beam theory for the case with no prestress ($P = 0$), prestress making the hoop stress zero in the flanges at $s = \pm\mathcal{L}$ ($P = P_\sigma$), prestress making the shear stress of the beam and membrane shell theories match at $s = \pm\mathcal{L}$ ($P = P_\tau$), and prestress minimising the wall bending moment at $s = 0$ ($P = P_m$), all determined considering LC3.

2. Assume that the longitudinal stress is determined by

$$\sigma_z = -\frac{P(\ell - z)x}{I}$$

and that the components σ_x, σ_y, and $\tau_{xy} = \tau_{yx}$ are zero.

3. Solve the remaining shearing stress components $\tau_{xz} = \tau_{zx}$ and $\tau_{yz} = \tau_{zy}$ using the soap-film method such that

$$\tau_{xz} = -\frac{\partial\phi}{\partial x}, \quad \tau_{yz} = \frac{\partial\phi}{\partial y} - \frac{Px^2}{2I} + \frac{\nu}{1+\nu}\frac{Py^2}{2I},$$

where ν is Poisson's ratio and $\phi = \phi(x, y)$ a stress function acting over the cross-section such that the curvature of ϕ is proportional to that of a pressurised soap bubble covering a hole with the same shape as the cross-section perimeter.

Even though we have studied the Griffith–Taylor theory in some detail, we do not fully understand why Torroja chose to use it because it would appear that the simpler Euler–Bernoulli beam theory is sufficient to calculate the bending moments in the wall of the structure. The Euler–Bernoulli beam theory also allows for the prestress to be a design parameter and provides the shape of the beam bending moment diagram.

4.2. Design calculations

The calculation document [45] solves sectional properties graphically and approximates integrals as sums. It considers a cantilever of length 9.5 m loaded with 2,750 kg self-weight and 4,960 kg water per metre length summed up as a point load at the tip.

4.2.1. Main reinforcement in the flanges

1. Bending moment at the cantilever support: (2,750 + 4,960) kg/m × 9.5^2 m^2 / 2 = 350,000 kgm.

2. Assume zero longitudinal stress at the top linearly increasing towards the bottom so that the stress resultant is position at 1/3 of the cross-section height measured from the bottom, or 0.95 m, resulting in 1.90 m lever arm between flange reinforcement and resultant. Then the bending moment equates a force couple worth 350,000 kgm/1.9 m = 184,000 kg each.

3. Place in each flange 4ϕ39 cables with a breaking load of 72,320 kg per cable, resulting in a safety factor of the main reinforcement of 72,320 kg/184,000 kg × 8 = 3.2.

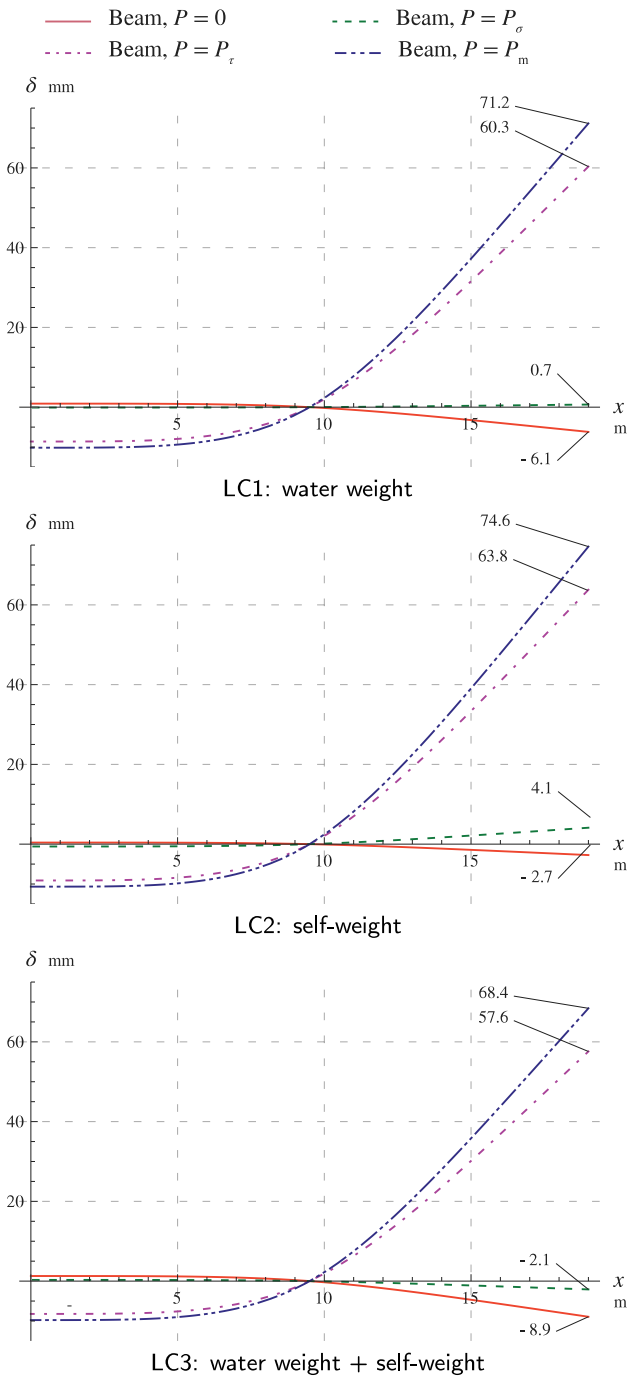

Fig. 11. Vertical displacement δ of neutral axis according to beam theory for a catenary cross-section.

4. Assume a fictitious maximum compression of 100 kg/cm^2 at the bottom and calculate the corresponding total compression volume 564,300 kg. Then recalculate to true maximum compressive stress σ_z as 350,000 kgm × 100 kg/cm^2 / 564,300 kg = 32.2 kg/cm^2. Torroja's assumed stress distribution is indicated in grey in the lower right plot in Fig. 9, deviating only slightly from our result.

5. In the end of the cantilever where only half the number of cables are laid, the compression is 92,000 kg. The centre of gravity for this section is 1.4 m and so the eccentric force is replaced with a moment 65,000 kgm and a force 92,000 kg positioned half way up, i.e. 1.45 m above the bottom. With cross-section area 11,685 cm^2 and moment of

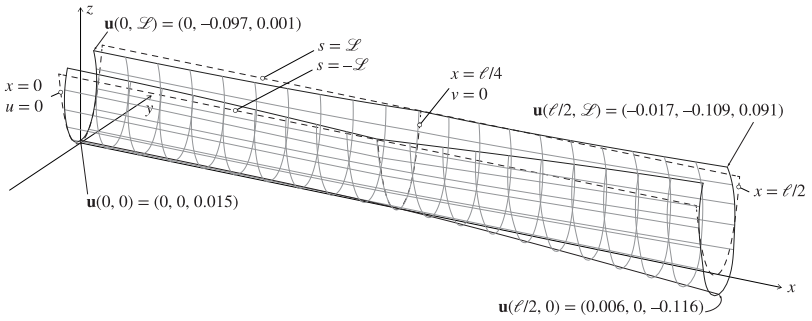

Fig. 12. Deformations [m] according to membrane shell theory for LC1: water weight. Deformations drawn scaled 5 times and undeformed shell outlined with dashed lines.

inertia 96,400 cm^4, the concrete compression in this section is

$$\frac{92,000}{11,685} \pm \frac{65,000 \times 100 \times 145}{96,400} = 7.9 \pm 10 \text{ kg/cm}^2.$$

4.2.2. Calculation of shear forces

1. Compute the shearing stresses τ_{xz} and τ_{yz} using the soap-film method at four points at the cross-section considering only the weight of the concrete.

2. Compute a stress resultant $t = \sqrt{\tau_{xz}^2 + \tau_{yz}^2}$ for each of the four points and combine with stress σ_z at the same points via Mohr's circle to determined principal stresses; max tension: 9.5 kg/cm^2; max compression: 32.0 kg/cm^2. Reinforcement 4.5ϕ15 bars per metre length resists the tension.

4.2.3. Calculations of bends in the wall

1. Use obtained shearing stresses combined with self-weight and hydrostatic pressure to compute the bending in the wall and recompute to a need for an additional 4.5ϕ15 bars per metre, resulting in a total of 9ϕ15 bars per metre.

2. Arrange the vertical reinforcement with an inclination according to Mohr's circle, slightly reduced towards the ends, see Fig. 3.

Note that at the tip of the cantilever, the reinforcement is arranged vertically and reduced to 9ϕ12 per metre, but there are not comments about this in the calculation document. Neither are there any mentions of the longitudinal reinforcement 8ϕ8 per metre in the channel wall shown in Fig. 3.

4.2.4. Tie rods

Use the resulting wall bending moment to design the tension ties connecting the two flanges: a ϕ25 bar every 4.75 m, each carrying a tension of 4,800 kg.

5. Summary

In this paper, we examine the structural action of Eduardo Torroja's prestressed concrete Alloz aqueduct completed in 1939. In particular, we address which simple theoretical approach would be the most suitable if you would design a similar structure today: the Euler–Bernoulli beam theory or the membrane theory of cylindrical shells. Furthermore, we review the Griffith–Taylor theory for the bending of cantilevers, which Torroja used to design the aqueduct.

The cylindrical membrane shell theory results in inadmissible infinite hoop stress if the considered cross-section curve has zero curvature. That is the case at the bottom of the Alloz aqueduct, whose cross-section is a 'cubic parabola'. In reality, if the wall is flexible enough in bending, the cross-section will change its geometry to relax such a stress concentration. However, this makes the membrane shell theory an invalid analysis approach for the Alloz aqueduct. To generalise the discussion and allow a comparison between the two theories, we have chosen to approximate the Alloz geometry using a catenary cross-section, which has everywhere non-zero curvature, and whose geometry deviates only slightly from Torroja's cubic parabola.

We have shown that, in general, it is possible to establish an equilibrium using either the cylindrical membrane theory or the Euler–Bernoulli beam theory for an aqueduct of similar cross-section as the Alloz aqueduct. The lower-bound theorem [1,2] then tells us that the structure will also find an equilibrium state. A specific level of prestressing is needed for equilibrium in the membrane shell theory, whereas it is satisfied for any level of prestressing in the beam theory.

With the beam theory, it is possible to prestress the aqueduct to such a degree that the wall bending moments are reduced to a minimum, making the aqueduct channel act predominantly by membrane stresses, as in the membrane shell theory. However, the level of prestress needed to do so is high, resulting in longitudinal compressive concrete stresses around the prestressing tension wires far beyond reasonable assumptions on concrete strength. Furthermore, such prestress would result in tensile concrete stresses at the bottom of the cross-section, with risks for water intrusion and corrosion as a result.

A level of prestress chosen so that the entire cross-section is put in longitudinal compression, just as Torroja did for his design, gives with the beam theory a plausible state of stress in the concrete wall and the flanges. In this paper, we have assumed that the prestress is proportional to the beam bending moment according to Eq. (26) producing a continuous variation in the pretension. This is a difference from Torroja's design assumption, with a step-wise variation of the prestressing proportional to the number of tension wires used: two at mid span and the tip of the cantilever versus four above the supports.

Upon comparing Torroja's results with ours, we can conclude that the Griffith–Taylor theory provides results that agree well with those obtained using the Euler–Bernoulli beam theory, bearing in mind the slight difference in geometry. The Griffith–Taylor theory implicitly applies the 'plane-section remain plane' assumption and is limited to cantilevers loaded with point loads at the tip. Furthermore, it is much more complicated to use than the Euler–Bernoulli beam theory.

It must be stressed that both the Euler–Bernoulli theory and the Griffith–Taylor theory likely underestimate the shear deformations of the Alloz aqueduct. This is reflected in the reduced accuracy of their results. Therefore, the theories should be used with caution and final designs checked using more refined approaches such as the finite element method. These checks should preferably include non-linear material models and time-dependent effects such as creep and relaxation.

6. Conclusion

Since the Alloz aqueduct does not have everywhere non-zero curvature, it cannot be analysed using the cylindrical membrane shell theory.

In general, whether or not a structure of this type acts as a shell depends upon the thickness of the wall. The thinner the wall, the more it act as a shell. The wall thickness of the Alloz aqueduct is sufficient for it to act mainly as a beam, and the beam theory gives a better approximation than the membrane shell theory.

Both the membrane shell theory and the Euler–Bernoulli beam theory produce a distribution of stresses within a cylindrical shell of

an appropriate shape which satisfy the equilibrium equations. Which is more appropriate in any given circumstance depends on the wall thickness and the boundary conditions.

CRediT authorship contribution statement

Alexander Sehlström: Conceptualization, Investigation, Methodology, Software, Validation, Visualization, Writing – original draft, Writing – review & editing. **Karl-Gunnar Olsson:** Methodology, Writing – review & editing, Supervision. **Chris J.K. Williams:** Conceptualization, Methodology, Writing – review & editing, Supervision.

Declaration of competing interest

The authors declare that they have no known competing financial interests or personal relationships that could have appeared to influence the work reported in this paper.

Acknowledgments

This research was enabled by joint financial support from Chalmers University of Technology Foundation and WSP.

Appendix. Simple beam with equal overhangs

Consider a simply supported aqueduct channel of length ℓ with equal overhangs of length $\ell/4$ at each side of the supports. Position the coordinate system so that $x = 0$ at mid span between the supports, see Fig. 8. Due to symmetry, we may consider only the half of the aqueduct, so we restrict our attention to where $0 \geq x \geq \ell/2$.

A.1. Cylindrical membrane shell theory

Combining Eqs. (10) and (12) gives the displacement field as

$$\left.\begin{aligned} u &= \frac{1}{Et}\left[\frac{x^3}{6}\left(\hat{n}_s'' + p_s'\right) + \frac{x^2}{2}C_1'' + \right. \\ &\qquad \left. x\left(C_2'' - \nu\hat{n}_s\right) + C_3\right] \\ v &= -\frac{1}{Et}\left[(1+\nu)\left(x^2\left(\hat{n}_s' + p_s\right) + 2xC_1'\right) + \right. \\ &\qquad \frac{x^4}{24}\left(\hat{n}_s^{(3)} + p_s''\right) + \frac{x^3}{6}C_1^{(3)} + \\ &\qquad \left.\frac{x^2}{2}\left(C_2^{(3)} - \nu\hat{n}_s'\right) + xC_3' - C_4\right] \\ w &= R\left(\frac{1}{Et}\left(\hat{n}_s - \nu\hat{n}_x\right) - \frac{\partial v}{\partial s}\right) \end{aligned}\right\} \tag{43}$$

where

$$\begin{aligned} \frac{\partial v}{\partial s} = -\frac{1}{Et}\Big[&(1+\nu)\left(x^2\left(\hat{n}_s'' + p_s'\right) + 2xC_1''\right) + \\ &\frac{x^4}{24}\left(\hat{n}_s^{(4)} + p_s^{(3)}\right) + \frac{x^3}{6}C_1^{(4)} + \\ &\frac{x^2}{2}\left(C_2^{(4)} - \nu\hat{n}_s''\right) + xC_3'' - C_4'\Big]. \end{aligned} \tag{44}$$

At mid-span ($x = 0$) and at the tip of the cantilever ($x = \ell/2$), the shear stress must be zero. Thus, from the second expression of Eq. (10), we get

$$C_1'(s) = \begin{cases} 0, & 0 \leq x \leq \dfrac{\ell}{4} \\ -\dfrac{\ell}{2}\left(\hat{n}_s' + p_s\right), & \dfrac{\ell}{4} < x \leq \dfrac{\ell}{2}. \end{cases} \tag{45}$$

At the end of the cantilever ($x = \ell/2$), the longitudinal stress $\hat{n}_x$ must be zero. Thus, from the first expression of Eq. (10) and with the usage of Eq. (45), we get $C_2'' = -\frac{\ell^2}{8}\left(\hat{n}_s'' + p_s'\right) - \frac{\ell}{2}C_1'' = \frac{\ell^2}{8}\left(\hat{n}_s'' + p_s'\right)$ for the cantilever. To solve for the central span, note that on either side of the support ($x = \ell/4$) the longitudinal stress must be the same. Therefor, using the previous result, $C_2'' = 0$ for the central span. Hence,

$$C_2''(s) = \begin{cases} 0, & 0 \leq x \leq \dfrac{\ell}{4} \\ \dfrac{\ell^2}{8}\left(\hat{n}_s'' + p_s'\right), & \dfrac{\ell}{4} < x \leq \dfrac{\ell}{2}. \end{cases} \tag{46}$$

Due to symmetry, the longitudinal displacement u at mid-span ($x = 0$) is 0. So, from the first expression in Eq. (43), we find $C_3 = 0$ for the central span. At either side of the support ($x = \ell/4$), the longitudinal displacement must be the same. Thus, using the previous results, $C_3 = -\ell^3/64\left(\hat{n}_s'' + p_s'\right)$ for the cantilever span. Hence,

$$C_3(s) = \begin{cases} 0, & 0 \leq x \leq \dfrac{\ell}{4} \\ -\dfrac{\ell^3}{64}\left(\hat{n}_s'' + p_s'\right), & \dfrac{\ell}{4} < x \leq \dfrac{\ell}{2}. \end{cases} \tag{47}$$

At the vertical support ($x = \ell/4$), assume no displacement in the hoop direction. Then, from the second expression in Eq. (43) and by noting that the hoop displacement must be the same on either side of the support, we find

$$C_4(s) = \begin{cases} c_{\text{mid}}(s), & 0 \leq x \leq \dfrac{\ell}{4} \\ -c_{\text{end}}(s), & \dfrac{\ell}{4} < x \leq \dfrac{\ell}{2}. \end{cases} \tag{48}$$

where

$$c_{\text{mid}}(s) = \frac{192\ell^2(2+\nu)\left(\hat{n}_s' + p_s\right) + \ell^4\left(\hat{n}_s^{(3)} + p_s''\right)}{6144}, \tag{49}$$

$$c_{\text{end}}(s) = \frac{192\ell^2(6+7\nu)\left(\hat{n}_s' + p_s\right) + 7\ell^4\left(\hat{n}_s^{(3)} + p_s''\right)}{6144}. \tag{50}$$

A.2. Beam bending theory

For the considered half of the beam, the beam bending moment is given by

$$M(x) = \begin{cases} -\dfrac{qx^2}{2}, & 0 \leq x \leq \dfrac{\ell}{4} \\ \dfrac{q\ell}{2}\left(x - \dfrac{\ell}{4}\right) - \dfrac{qx^2}{2}, & \dfrac{\ell}{4} < x \leq \dfrac{\ell}{2}, \end{cases} \tag{51}$$

where $q = g\left(A_c\rho_c + A_w\rho_w\right)$ is the uniformly distributed load per unit length.

The vertical displacement of the neutral axis is

$$\delta(x) = \begin{cases} -\dfrac{q(\ell - 4x)}{6144E\tilde{I}}f_{\text{mid}}(x), & 0 \leq x \leq \dfrac{\ell}{4} \\ -\dfrac{q(\ell - 4x)}{6144E\tilde{I}}f_{\text{end}}(x), & \dfrac{\ell}{4} < x \leq \dfrac{\ell}{2}, \end{cases} \tag{52}$$

where

$$f_{\text{mid}}(x) = 15\ell^3 - 68\ell^2x + 112\ell x^2 - 64x^3, \tag{53}$$

$$f_{\text{end}}(x) = 7\ell^3 - 68\ell^2x + 112\ell x^2 - 64x^3. \tag{54}$$

References

[1] Calladine CR. Plasticity for engineers. Woodhead Publishing; 2000.
[2] Hillerborg A. Strip method design handbook. London, New York: E & FN Spon; 1996.
[3] Sutherland RJM. Historic Concrete: Background to appraisal. London Reston, VA: Thomas Telford; 2001.
[4] Ochsendorf J, Antuña J. Eduardo Torroja and "Cerámica Armada". In: Huerta S, editor. In: Proceedings of the first international congress on construction history, vol. III, Madrid: Instituto Juan de Herrera; 2003, p. 1527–36.
[5] Addis B. Building: 3000 years of design engineering and construction. Phaidon; 2007.
[6] Corres H, Leon J. Eminent structural engineer: Eduardo Torroja (1899–1961). Struct Eng Int 2012;22(4):581–4. http://dx.doi.org/10.2749/101686612X13363929517938.

[7] Billington DP. The founding of the IASS: Eduardo Torroja nad the context until 1959. In: Mungan I, Abel JF, editors. Fifty years of progress for shell and spatial structures : In celebration of the 50th anniversary jubilee of the IASS (1959–2009). Madrid: International Association for Shell and Spatial Structures; 2011, p. 3–12.

[8] Antuña J. Physical models: Their historical and current use in civil and building engineering design. In: Eduardo Torroja and his use of models up to 1936. Ernst, Wilhelm & Sohn; 2020, p. 321–43.

[9] Antuña J. Physical models: Their historical and current use in civil and building engineering design. In: Eduardo Torroja and his use of models from 1939. Ernst, Wilhelm & Sohn; 2020, p. 477–510.

[10] Lozano-Galant JA, Payá-Zaforteza I. Structural analysis of Eduardo Torroja's Frontón de Recoletos' roof. Eng Struct 2011;33(3):843–54. http://dx.doi.org/10.1016/j.engstruct.2010.12.006.

[11] Torroja E. Mercado de algeciras. Inf Constr 1962;14(137):51–8. http://dx.doi.org/10.3989/ic.1962.v14.i137.4932.

[12] Moragues JJ, Paya-Zaforteza I, Medina O, Adam JM. Eduardo Torroja's Zarzuela Racecourse grandstand: Design, construction, evolution and critical assessment from the structural art perspective. Eng Struct 2015;105:186–96. http://dx.doi.org/10.1016/j.engstruct.2015.10.008.

[13] Torroja E. Hipódromo de la Zarzuela. Inf Constr 1962;14(137):19–38. http://dx.doi.org/10.3989/ic.1962.v14.i137.4930.

[14] Torroja E. Frontón recoletos. Inf Constr 1962;14(137):41–50. http://dx.doi.org/10.3989/ic.1962.v14.i137.4931.

[15] Cabello A, Paya-Zaforteza I, Adam JM. Non-linear analysis of Eduardo Torroja's Frontón de Recoletos' roof using a discrete reinforcement approach. Eng Struct 2014;80:406–17. http://dx.doi.org/10.1016/j.engstruct.2014.08.044.

[16] Torroja E. Philosophy of structures. Berkeley: University of CaliforniaPress; 1958.

[17] Torroja E. The structures of Eduardo Torroja: An autobiography of engineering accomplishment. New York: F.W. Dodge Corporation; 1958.

[18] Johnson RD. The hydrostatic chord : With discussion of its application in the design of large pipes of reinforced concrete. In: Presented at the spring meeting, Atlantic City, 1910, of the American society of mechanical engineers. 1910. p. 521–5.

[19] Levien R. The elastica: A mathematical history. Technical report UCB/EECS-2008-103, Electrical Engineering and Computer Sciences, University of California at Berkeley; 2008.

[20] Foster RM, Ibell TJ. A numerical solution for the shape of fabric-formed concrete structures. Structures 2016;8:17–24. http://dx.doi.org/10.1016/j.istruc.2016.08.003.

[21] Rouhi A. Historic reinforced concrete in Alberta : Analysis and conservation of two structures [Ph.D. thesis], Calgary, AB: University of Calgary; 2018, http://dx.doi.org/10.11575/PRISM/33162, URL http://hdl.handle.net/1880/108822.

[22] Manz DH, Loov RE, Webber J. Brooks aqueduct. Can J Civil Eng 1989;16(5):684–92. http://dx.doi.org/10.1139/l89-102.

[23] Timoshenko S, Woinowsky-Krieger S. Theory of plates and shells. 2nd ed.. McGraw-Hill book company; 1959.

[24] Torroja E. Acueducto de tempul. Inf Constr 1962;14(137):135–40. http://dx.doi.org/10.3989/ic.1962.v14.i137.4943.

[25] Lozano-Galant JA, Paya-Zaforteza I. Analysis of Eduardo Torroja's tempul aqueduct an important precursor of modern cable-stayed bridges, extradosed bridges and prestressed concrete. Eng Struct 2017;150:955–68. http://dx.doi.org/10.1016/j.engstruct.2017.07.057.

[26] Gran Enciclopedia de Navarra. Alloz, acueducto de. 2020, http://www.enciclopedianavarra.com/?page_id=3103. [Accessed 15 October 2020].

[27] Antuña J. Las estructuras de edificación de Eduardo Torroja Miret [Ph.D. thesis], Arquitectura; 2003, URL http://oa.upm.es/1348/.

[28] Torroja E. Secciones y detalles de los acueductos. Escala 1:50. No 358.226,4. Archivo Torroja, CEHOPU-CEDEX, ETM-179-45-028. 1939.

[29] Torroja E. Acueducto principal. Escala 1:250. No 358.225,1. Archivo Torroja, CEHOPU-CEDEX, ETM-179-45-027. 1939.

[30] Torroja E. Pantano de alloz. Sección del acueducto. No 2. Escala 1:50. Archivo Torroja, CEHOPU-CEDEX, ETM-179-45-205.

[31] Torroja E. Acueducto de alloz. Inf Constr 1962;14(137):143–8. http://dx.doi.org/10.3989/ic.1962.v14.i137.4944.

[32] Torroja E. The alloz aqueduct, Spain: A prestressed watertight structure. In: Concrete and constructunal engineering, vol. 43, 1948, p. 315–6.

[33] Finsterwalder U. Die theorie der zylindrischen Schalengewölbe system Zeiss-Dywidag und ihre anwendungauf die Grossmarkthalle in Budapest, 1. Zurich, Switzerland: IABSE Publications; 1932, p. 127–52. http://dx.doi.org/10.5169/seals-712.

[34] May R. Shell sellers. The international dissemination of the Zeiss-Dywidag system 1923–1939. In: Friedman D, editor. In: Proceedings of the 5th international congress on construction history, vol. 2, Chicago; 2015, p. 557–64.

[35] Kazinczy GV. Beräkning av cylindriska skal med hänsyn till den armerade betongens egenskaper. Betong 1949;(23):239–61.

[36] Elishakoff I. Who developed the so-called Timoshenko beam theory? Math Mech Solids 2020;25(1):97–116. http://dx.doi.org/10.1177/1081286519856931.

[37] Griffith AA, Taylor GI. The problem of flexure and its solution by the soap-film method. Adv Com aeronautics, Tech report (British) No. 399, 3, 1917, p. 950–69.

[38] Martínez MM. Origin of equilibrium methods applied to the structural calculation of long cylindrical shells. Constr Hist 2019;34(2):53–74, URL https://www.jstor.org/stable/27041601.

[39] Kazinczy GV. Die plastizitat des eisen betons. Beton Eisen 1933;32(5):74–80.

[40] Kazinczy GV. Critical observation on the theory of plasticity. In: Proc., int. association for bridge and structural engineering congress, vol. 2, Zürich, Switzerland: International Association for Bridge and Structural Engineering; 1936, p. 56–69.

[41] Kaliszky S, Sajtos I, Lógó BA, Lógó JM, Szabó Z. Gábor Kazinczy and his legacy in structural engineering. Period Polytech Civ Eng 2015;59(1):3–7. http://dx.doi.org/10.3311/PPci.8016.

[42] Bauchau OA, Craig JI. Thin-walled beams. In: Structural analysis. Dordrecht: Springer Netherlands; 2009, p. 297–391. http://dx.doi.org/10.1007/978-90-481-2516-6_8.

[43] Torroja E. Aqueducto de alloz=the aqueduct of alloz in Spain. Archivo Torroja, CEHOPU-CEDEX, TC-30. 1947.

[44] Torroja E. Teoría del método de la lámina de jabón. Archivo Torroja, CEHOPU-CEDEX, ETM-179-45-004. 1939.

[45] Torroja E. Calculo del acueducto de alloz. Archivo Torroja, CEHOPU-CEDEX, ETM-179-45-003. 1940.

[46] Timoshenko SP, Goodier JN. Theory of elasticity. 2nd ed.. New York and London: McGraw-Hill book company, inc.; 1951.